



**CHALMERS**  
UNIVERSITY OF TECHNOLOGY

## **Sample preparation and measurement strategies for characterisation of lignocellulose fibres using carbon K-edge spectro-microscopy**

Downloaded from: <https://research.chalmers.se>, 2026-04-16 05:44 UTC

Citation for the original published paper (version of record):

Björn, L., Olsson, M., Westman, G. et al (2026). Sample preparation and measurement strategies for characterisation of lignocellulose fibres using carbon K-edge spectro-microscopy. *Cellulose*, 33(2): 649-664.  
<http://dx.doi.org/10.1007/s10570-025-06869-1>

N.B. When citing this work, cite the original published paper.



# Sample preparation and measurement strategies for characterisation of lignocellulose fibres using carbon K-edge spectro-microscopy

Linnea Björn · Martina Olsson · Gunnar Westman · Agnieszka Ziolkowska · Jonathan Avaro · Benjamin Watts · Aleksandar Matic · Marianne Liebi

Received: 9 May 2025 / Accepted: 16 November 2025 / Published online: 10 December 2025  
© The Author(s) 2025

**Abstract** Cellulose fibres are a sustainable alternative for development of new materials and with chemical modifications the material properties can be tailored for its intended application. To understand the impact of a modification characterisation techniques that reveal where the chemical alterations occur across the fibre are needed. Here we showcase how X-ray spectro-microscopy around the carbon K-edge can provide spatially resolved images of the

chemical content of cellulose fibres and investigate the effect of different sample preparation strategies on the resulting data quality. We show that that one can spatially separate different lignin compositions over a single thermomechanical pulp fibre. The sample preparation is key for a successful experiment and requires sectioning of thin slices (~100 nm) of the sample which can be achieved by microtome sectioning. The effect of different embedding materials, including epoxies, cryo-embeddings with water and sucrose and elemental sulphur, is evaluated. The results show that epoxy embeddings are beneficial for homogenous sectioning, which is an advantage for imaging, while embedding strategies without carbon

---

Linnea Björn and Martina Olsson contributed equally.

---

**Supplementary Information** The online version contains supplementary material available at <https://doi.org/10.1007/s10570-025-06869-1>.

---

L. Björn · M. Olsson · A. Matic · M. Liebi (✉)  
Department of Physics, Chalmers University of Technology, 412 96 Gothenburg, Sweden  
e-mail: marianne.liebi@psi.ch

L. Björn · G. Westman · M. Liebi  
FibRe-Centre for Lignocellulose-Based Thermoplastics, Department of Chemistry and Chemical Engineering, Chalmers University of Technology, 412 96 Gothenburg, Sweden

G. Westman  
Department of Chemistry and Chemical Engineering, Chalmers University of Technology, 412 96 Gothenburg, Sweden

A. Ziolkowska  
Chemistry Department, Umeå Center for Electron Microscopy, Umeå University, S-90187 Umeå, Sweden

J. Avaro  
Center for X-Ray Analytics, Swiss Federal Laboratories for Materials Science and Technology, Lerchenfeldstrasse 5, 9014 EmpaSt. Gallen, Switzerland

B. Watts · M. Liebi  
Centre for Photon Science, Paul Scherrer Institut, 5232 Villigen PSI, Switzerland

A. Matic  
Wallenberg Wood Science Centre, Chalmers University of Technology, 412 96 Gothenburg, Sweden

M. Liebi  
Institute of Materials, Ecole Polytechnique Fédérale de Lausanne (EPFL), 1015 Lausanne, Switzerland

species, such as elemental sulphur or cryo-embedding with water, is better for evaluation of the chemical content in the fibre due to less overlap in the spectral signal from the embedding material. We also present measurement strategies for efficient data collection that minimise the inflicted radiation dose to provide guidelines for performing synchrotron-based spectro-microscopy around the carbon K-edge to characterise cellulose fibres.

**Keywords** Thermomechanical pulp · Sample preparation · STXM · NEXAFS · Embedding strategies · Microtome sectioning · Fibre materials

## Introduction

Lignocellulose fibres are versatile material building blocks used in a wide range of applications, including new materials and commodity products such as paper, packaging, and textiles. It is a renewable resource and the most abundant polymer on earth, resulting in a highly sustainable alternative. The pulp and paper industry produces different qualities of pulps, and one of them is thermomechanical pulp, which is produced by mechanical processing of wood chips. In thermomechanical pulp, all naturally occurring components of wood, such as lignin, cellulose, and hemicellulose, are preserved and thus no chemical after treatments are applied to extract different components (Mleziva et al. 2012). This makes the material cheaper and more environmentally friendly compared to using pure lignin or cellulose. The final fibre has a high lignin content primarily situated on the outer region of the fibre (Fromm et al. 2003; Mleziva et al. 2012). Biopolymers like lignin and cellulose have a diverse structure which is dependent on the plant-source of the fibre and the chemical composition can therefore deviate slightly between samples, however the common characteristic for lignin is a phenolic structure built from aromatic monomers while the cellulose is a polysaccharide consisting of a linear chain of glucose molecules (Karunakaran et al. 2015). Previous studies have shown that by introducing chemical modification into thermomechanical pulp, the material properties can be tailored (Lahtinen et al. 2021). However, since thermomechanical pulp is a complex material, consisting of lignin, hemicellulose and cellulose, the material properties obtained heavily depend on which

of the components that is most prone to react during modification. For example, by modifying the hydrophilic cellulose the compatibility between thermomechanical pulp and a polymer matrix can be improved (Mertens et al. 2017). On the other hand, selectively modifying lignin could preserve or even lower its thermal processing temperature, potentially enabling fibre extrusion (Lahtinen et al. 2021), a method that is severely hindered by the degradation of fibres during processing. However, there is no good understanding or systematic studies in the literature on how reaction conditions affect where modifications occur in the fibre.

To characterise where the modifications occur across the fibre, methods to study the spatial distribution of chemical composition on the nano- to micron scale are needed. Spectroscopy-based imaging techniques such as FTIR-AFM and X-ray spectro-microscopy can provide spatially resolved chemical information at the nanoscale (Dazzi and Prater 2017; Watts and Ade 2012). FTIR-AFM enables mapping of functional groups under ambient conditions, whereas X-ray spectro-microscopy, offers greater chemical sensitivity and high chemical contrast but requires synchrotron radiation and more involved sample preparation. Synchrotron-based spectro-microscopy combines X-ray scanning transmission microscopy and spectroscopy to provide the high resolution imaging with high chemical contrast (Watts and Ade 2012). By coupling near-edge X-ray absorption fine structure (NEXAFS) spectroscopy with scanning transmission X-ray microscopy (STXM), imaging is made through raster scanning the sample over a focused beam, which can reach spatial resolutions down to tens of nanometres. Thereby, spectro-microscopy at energies corresponding to the carbon K-edge (280–320 eV) presents high potential for detailed characterization of lignocellulose fibres to detect distribution of components and locations of chemical modifications. However, the measurements present challenges due to demanding sample preparation of thin slices, which are required to ensure sufficient transmission because of the strong absorption of carbon-based materials in this X-ray energy range. Cellulose-based samples are typically prepared with a thickness of 90–200 nm to provide optimal transmission, maintaining about 30–60% of the incident X-ray intensity which is important to obtain high-quality spectral data (Karunakaran et al. 2015; Watts et al.

2022). A common approach for preparing thin samples involves using an embedding and cutting slices with a microtome. However, many embeddings contain carbon, which can introduce spectral overlaps in NEXAFS measurements, potentially interfering with an accurate analysis. Other challenges are associated with the data acquisition, as radiation damage is often a critical factor that needs to be mitigated. Exposure to intense X-ray radiation can lead to structural and chemical alterations in a sample, leading to variations in the acquired spectra. Radiation damage has been reported to be significant in polymer materials, where bond breakage, mass loss, and radical formation can occur (Coffey et al. 2002; Beetz and Jacobsen 2003), and the sensitivity to radiation damage can be affected by the embedding material used during the sample preparation (Beetz and Jacobsen 2003; Wang et al. 2009; Zhang et al. 2019). The high flux-density of the focused beam and the low X-ray energies makes this particularly critical in spectro-microscopy.

In this paper, we present a study of different sample preparation protocols for performing spectro-microscopy of fibres around the carbon K-edge. We describe the results of five sample preparation protocols for preparing thin slices using microtoming with different embedding strategies from the perspective of three aspects crucial to acquiring high-quality spectro-microscopy data: (1) quality of the cut slices (2) spectral overlaps and (3) exacerbated radiation sensitivity. In addition, we discuss measurement strategies for collecting data in an efficient way to provide a compromise of spectral and spatial resolutions to optimise measurement time at synchrotrons and mitigate radiation damage. The aim is to provide guidelines for performing synchrotron spectro-microscopy to characterise cellulose-based fibres and promote increased success rate and utilisation of such measurements.

## Methods

### Material

Thermomechanical pulp (TMP) used for the measurement was produced by processing wood chips using heat and mechanical refining. The TMP fibres utilised in the study were obtained from StoraEnso Hyltebruk, Sweden and were derived from Norway spruce (*Picea*

*abies*). Fibre analysis of the TMP, performed using a Kajaani FS300, gave a respective mean fibre length, width, and fines distribution of 3.2 mm, 35  $\mu\text{m}$ , and 3% (Hosseini et al. 2021). TMP has been reported to have 50 wt.% of polysaccharides and ca. 30–35 wt.% lignin (Kangas et al. 2007).

### Sample preparation strategies

**Spurr epoxy sample preparation protocol:** Spurr resin with ERL-4221D formulation was used. ERL-4221D (Epoxy-cyclohexylmethyl-3,4-epoxy-cyclohexylcarboxylate) is a cycloaliphatic epoxy resin that is typically used as an embedding medium for electron microscopy. The epoxy was polymerised at 65 °C overnight before cutting at ambient conditions.

**Cycloamine-based epoxy sample preparation protocol (CBE):** Epoxy resin derived from a 1:1 mixture of 4,4-methylenebis(2-methylcyclohexylamine) and 2-[2,2-bis(oxiran-2-ylmethoxymethyl)butoxymethyl]oxirane was used based on Späth et al. (2015). The epoxy was polymerised at 65 °C overnight before cutting at ambient conditions (Steudel et al. 2003; Lehmann et al. 2005; Noguchi et al. 2020).

**Sucrose sample preparation protocol:** The fibres were immersed in a 2 M sucrose solution. After immersion, the samples were sandwiched between pieces of plastic and filter paper to make handling the fragile material easier while sectioning in cryogenic conditions at -160 °C.

**Water sample preparation protocol:** The fibres were immersed in Milli-Q water. After immersion, the samples were sandwiched between pieces of plastic and filter paper to make handling the fragile material easier while sectioning in cryogenic conditions at -160 °C.

**Sulphur sample preparation protocol:** Elemental sulphur was used as embedding material, adapted from Lehmann et al. (2005) and Noguchi et al. (2020). Sulphur (0.75 g) was placed on a tray of aluminium foil at 170 °C for 2 min until the sulphur became viscous and reddish-brown. A lower temperature was chosen compared to Lehmann et al. to avoid heat induced damage of the mixture. The aim was for  $S_8$ -rings to open and form diradicals in the elemental sulphur, which happens above 159 °C. The radicals then polymerise into long chains which increases the viscosity (Steudel et al. 2003). The aluminium trays were then placed in liquid nitrogen for a quenching

step. During this step, the sulphur becomes an amorphous solid. It was then left to heat up at ambient conditions for about 2–4 min until it turned into a viscous state. Cellulose fibres were carefully pressed into the sulphur with tweezers. The optimum consistency for this step only lasted for about 10–30 s, after which the amorphous sulphur converts to a microcrystalline but still plastic state. The sulphur-embedded cellulose fibres were then transferred to an ultramicrotome and cut at cryogenic conditions at  $-160\text{ }^{\circ}\text{C}$ .

All sample preparation protocols used ultramicrotome Leica EM FC7 to cut samples into 150 nm thin sections. After the sectioning, the sample slices were placed on silicon nitride,  $\text{Si}_3\text{N}_4$ , membranes with a thickness of 100 nm. All samples were stored in room temperature after slicing prior to the measurements.

### STXM

The STXM measurements were performed at the PolLux beamline of the Swiss Light Source (SLS)

synchrotron at the Paul Scherrer Institute in Villigen, Switzerland. The detailed beamline layout is described by Raabe et al. (2008). A higher order suppressor (Frommherz et al. 2010) was used to ensure probing a pure spectrum as higher order light will distort the spectra. A focused soft X-ray beam with a beam size of  $\geq 30\text{ nm}$  was used to raster scan across the samples, collecting the transmission value in each point using a photomultiplier tube (PMT), coupled with a phosphor screen. First, a single energy measurement on the carbon post edge at 330 eV, as indicated in Fig. 1b, c, was used to locate the fibres on the support membrane. Once regions of interest were determined, NEXAFS spectra were collected by a stack of image measurements in the energy range of 280–350 eV, which corresponds to the collection of a carbon K-edge spectrum at each image pixel. The energy step size varied from 0.1 eV around the absorption edge to 1 eV in the post-edge region. To evaluate radiation damage, spectra were collected by focusing the X-ray beam on the sample and then repeatedly measuring a line scan of 50 points with

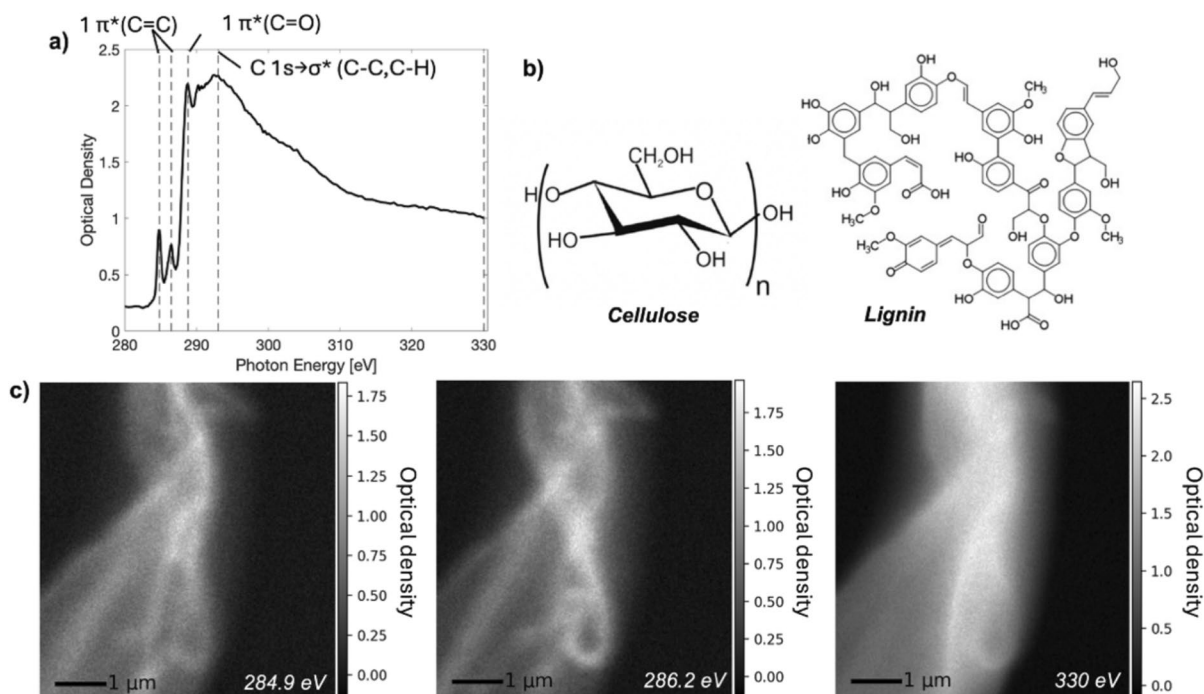


**Fig. 1** a Characteristic NEXAFS spectrum from a lignocellulose fibre showing resonance energies from both lignin and cellulose components. b Model structure of cellulose and lignin based on (Adler 1977). c Images collected at the reso-

nance energies for lignin (284.9 eV, 286.2 eV), and at the post-edge (330 eV) which is sensitive to the electron density of the section and highlights the entire fibre

an increment in exposure time of 5 or 20 ms, respectively. The line scan was repeated in the same position three times and the spectral changes were compared after the beam exposure.

MANTiS analysis software was used to analyse the X-ray spectro-microscopy data (Lerotic et al. 2014). The transmission of X-ray photons through the fibres measured were converted to optical density,  $OD = -\ln(I/I_0)$ , where  $I_0$  and  $I$  are the incident and transmitted photon count. The incident flux is measured via an empty region on the support membrane. Normalisation was performed to compare spectra by dividing with the post-edge measurement, which is sensitive to the electron density, to correct for density and thickness variations.

## Results

Figure 1 showcases a spectro-microscopy measurement around the carbon K-edge of a cellulose fibre from thermomechanical pulp (TMP). Figure 1a shows the NEXAFS spectrum around the carbon K-edge showing characteristic signatures from both lignin and cellulose. Two peaks are seen at 284.9 eV and 286.2 eV characteristic of the C 1  $s \rightarrow 1 \pi^*$  (C=C) transition of aromatic (C-H) and phenolic carbons (C-O), respectively, and at 288.7 eV a peak corresponding to the C 1  $s \rightarrow 1 \pi^*$  (C=O) transition of carboxylic carbon (Karunakaran et al. 2015). These functional groups are all characteristic of lignin and can therefore be used to identify the distribution of lignin across the fibre. The peak at 290.4 eV is related to the aliphatic C-H carbons, and the broad peak at 293 eV to C 1  $s \rightarrow \sigma^*$  transitions in aromatic and aliphatic carbons present in both cellulose, lignin, and hemicellulose (Karunakaran et al. 2015). Example structures of cellulose and lignin are shown in Fig. 1b. The cellulose fibres also contain hemicellulose, however, due to the similarity in the chemical structure to cellulose it is not distinguished in the measurement.

Figure 1c shows three optical density images collected at energies corresponding to the characteristic peaks of lignin (284.9 eV, 286.2 eV) and the post-edge (330 eV), which relates to thickness variations across the fibre as this energy is sensitive to overall electron density. The fibre was imaged using a focused 30 nm beam with a step size of 30 nm. A high optical density at the resonance energies of aromatic

(284.9 eV) and phenolic carbons (286.2 eV) identifies a high lignin content and visualise how the lignin is twisting around the filament. This is in agreement with lignin working as a glue between individual fibres in lignocellulose (Akin et al. 2010). Comparing the two images with contrast from aromatic and phenolic carbons reveals that there is a difference in the spatial intensity distribution between the two lignin peaks over the fibre. This can be related to a variation in the relative fraction of the monomers p-coumaryl, coniferyl, or sinapyl monomers which have different amount of phenolic groups (Karunakaran et al. 2015) and reveals a spatial variation in chemical composition of the lignin over the cellulose fibre. The spatial variation of the peak intensities could also indicate molecular orientation (via linear dichroism), but this is unlikely to be significant in this case due to the amorphous nature of the material.

## Comparison of the quality of sample sectioning

Sectioning quality varied between the different sample preparation protocols (Fig. 2). From a sectioning perspective, epoxy-based methods such as the Spurr- or cycloamine-based epoxy sample preparation protocols, were advantageous since they provided the easiest sectioning process, resulting in large, uniform sections with well-dispersed fibres and easy sample transfer to the support membrane (Fig. 2a). On the contrary, immersion of the fibres in a liquid, like water or sucrose, and sectioning at cryogenic conditions caused issues with fibre clustering (Fig. 2b), making it difficult to investigate individual fibres. The sucrose embedding protocol allowed for easy sectioning, whereas the water-embedded samples were the most challenging to section. Under cryogenic conditions, the water-embedded samples turned very brittle, making it difficult to create regular sections. To overcome this, a high cutting speed was needed, and multiple attempts were required to obtain satisfactory sections. The sulphur embedding protocol posed the greatest challenges during the embedding phase, as the success of embedding was highly sensitive to temperature and timing of each embedding step. Once the embedding was successful, the sectioning was straightforward, creating sectioning ribbons of intermediate sizes (Fig. 2c).

The sulphur embedding caused additional problems during the measurements. Under vacuum

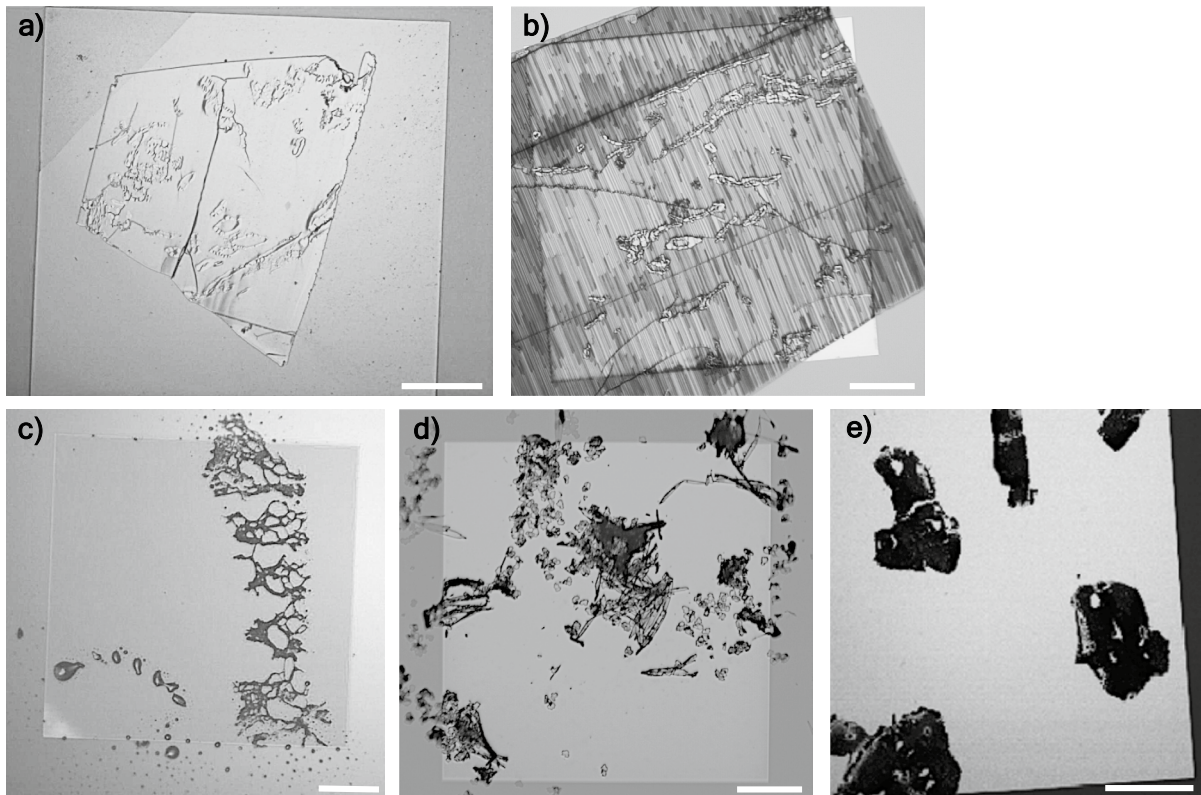


**Fig. 2** Microscopy images of sectioned samples. **a** Spurr epoxy embedding **b** Cycloamine-based epoxy embedding **c** Cryo-embedding with sucrose, **d** Cryo-embedding with water **d** Sulphur embedding. The scale bar corresponds to 0.2 mm

conditions, the sulphur began to evaporate, leaving the fibre samples exposed. This resulted in fibres moving and detaching from the support membrane during measurements. We hypothesize that this occurred due to charge accumulation on the sample surface. To mitigate this effect, coating the support membrane with a conductive material, such as graphene or a thin metal layer, could help dissipate the charge. Alternatively, sandwiching the fibre samples between two separate membranes may provide mechanical stability and prevent displacement.

A quality criterion for sectioning is to achieve a homogenous thickness across the samples. To evaluate the sample thickness, measurements were taken at the carbon post edge, 320–330 eV (Fig. 3). The most homogenous profiles were achieved when epoxy was used, showing a low variation of sample thickness over larger areas, Fig. 3a–b. This is emphasised when plotted with the same scalebar as the other embeddings, where it is difficult to differentiate between

sample and the embedding (Fig. 3c and 3d). This is due to similar density of carbon content in the epoxy and the fibre samples. In the non-epoxy-based approaches, the post-edge provided a clear signal of where the fibres were located. However, within the fibres thickness variations were observed. The water embedded sample showed larger variations in optical density compared to the epoxy-based approaches and using sulphur and sucrose embedding even larger variations of optical density, i.e. larger variation in sample thickness, was found.

#### Comparison of signal quality

The measured NEXAFS spectrum includes the signal from all material illuminated by the X-ray beam. In the ideal case the embedding material would only surround the fibres, however it is not unlikely that some of it will penetrate the fibres or that over the thickness of a section both fibre and embedding material

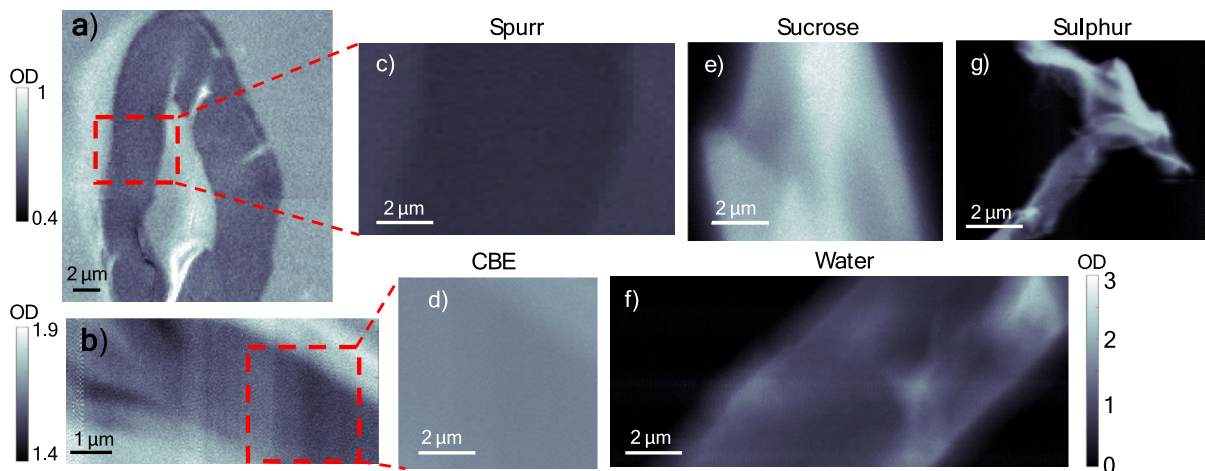


**Fig. 3** Images taken at the carbon post edge of fibres using **a, c** Spurr epoxy, **b, d** Cycloamine-based epoxy, **e** Sucrose, **f** Water, and **g** Sulphur sample preparation protocols. The fig-

ure shows larger areas of epoxy embedded samples in **a-b** and plotted with a different scale bar of the optical density (OD) compared to **c-d**

will be present. In these cases, the absorption spectrum will be a superposition of the two materials. For fibres embedded in epoxy and sucrose, the carbon species in the embedding materials can therefore contribute to the spectrum and complicate the analysis due to overlapping signals. The more chemically different a carbon-based embedding material is, the less overlap with the signal can be expected. Spectra from fibres embedded in water and elemental sulphur are expected to have minimal spectral overlaps since no carbon-based materials are included in the embedding.

Figure 4a-e shows a representative spectrum acquired from embedded fibres prepared with each sample protocol (black) together with a reference measurement (grey) of the embedding materials only. Figure 4f shows a comparison of the spectra normalised at the-post edge to compensate for variation in thickness from embedded fibres prepared through each preparation protocol. As expected, the fibres prepared with the water and sulphur embedding display similar spectra, reflecting the chemical composition of the cellulose fibres. The two aromatic peaks from the lignin at 284.9 eV and 286.2 eV are clearly visible and are comparably pronounced in the two samples. Similarly, the peak at 288.7 eV and the shape of the broad transition at 293 eV for C 1s  $\rightarrow \sigma^*$  transitions of aromatic and aliphatic carbons remain consistent. The spectrum from sucrose embedded

fibres differs slightly from spectra from fibre with the water and sulphur embedding, the relative intensities between the aromatic lignin peaks is lower compared to the broad peak at 293 eV for C 1s  $\rightarrow \sigma^*$  transitions of aromatic and aliphatic carbons. Since the sample has been diluted with sucrose, the measured spectrum is a linear combination of the component materials and hence shows a stronger signal from saccharides relative to the lignin due to the sucrose contribution which is indistinguishable from the cellulose contribution. A similar phenomenon can be observed for fibres with the cycloamine-based epoxy embedding, where the spectrum also shows a lower relative signal from lignin, which can be explained by the contribution from the aliphatic carbon species in the embedding material. The spectrum from the sample prepared with the Spurr epoxy embedding displayed the strongest spectral overlap from the embedding, Fig. 4a. Here, the entire shape of the spectrum is modified due to the superposition of the resonance peaks around  $\sim 284.8$  and  $\sim 288$  eV, complicating the analysis further due to difficulties of decoupling the different contributions. One additional problem which can occur are contaminations of salt species that overlap with the carbon K-edge spectra. This was observed in the sample prepared with the water embedding protocol, Fig. S1. The contamination is identified by the two sharp peaks at 296.8 eV and 299 eV which corresponds to the L-edge of potassium (Deslattes et al.

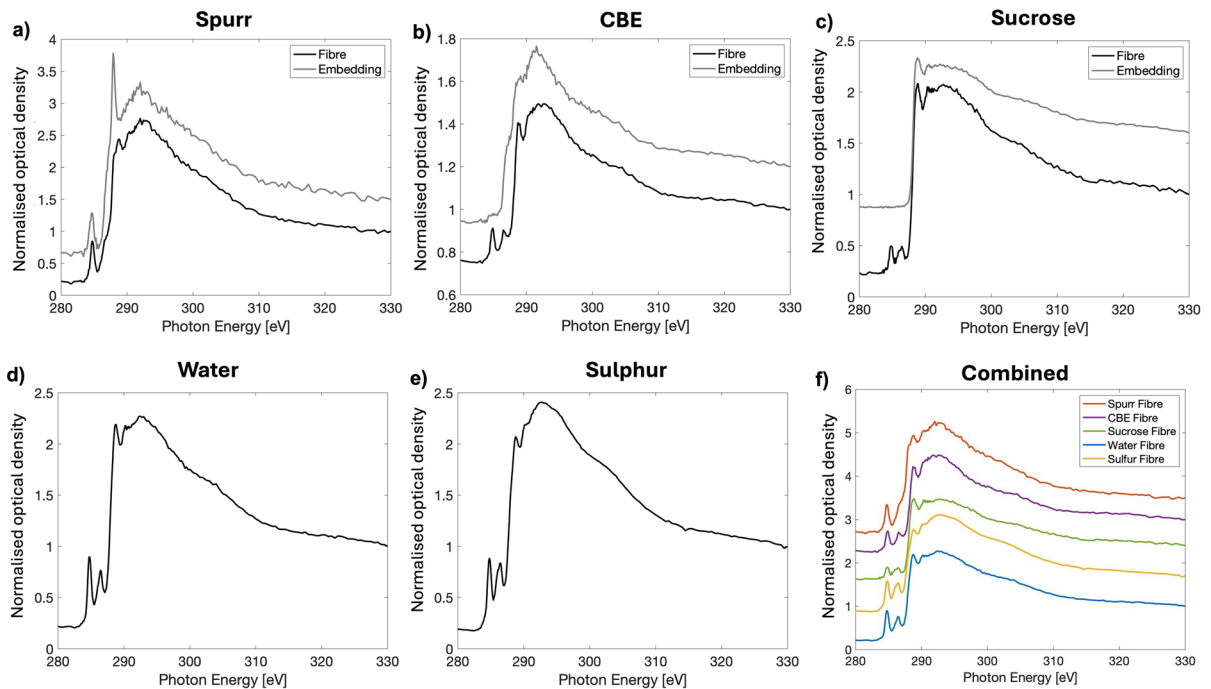


**Fig. 4** a–e Spectra from embedded fibres and embedding materials prepared through the different sample preparation protocols. Spectra acquired from fibres (black) together with

the reference of each embedding material (grey), offset for clarity. **f** Normalised spectra from the fibres prepared through each preparation protocol. The spectra are offset for clarity

2003) and reveals salt contamination. Such impurities may arise due to residue ions and are also common impurities following manual handling due to the salt in sweat and can therefore be found locally within prepared materials.

#### Comparison of radiation damage

To study radiation damage, line scans of 50 points were repeatedly measured with an exposure time of 5 or 20 ms, respectively. By repeated measurements in the same spot, spectral changes can be evaluated as a function of beam exposure to identify beam damage in the different samples. The sensitivity for radiation damage may differ between the embeddings as reactive species from the embedding material may react under the beam energy. Conductivity of the embedding material may also reduce static build-up which can help mitigate reactions in the samples after dose exposure. Figure 5 shows radiation damage tests for all sample preparation protocols with 20 ms increment. The light colored spectrum is the average signal from the first measurement with 20 ms exposure

and the gradually darker colored spectra shows the second and third measurement with an exposure time of 40 and 60 ms in total. In the case of epoxy-based sample preparation protocols, pure epoxy without any embedded fibres was also measured, shown as insets. Figure S2 shows the radiation damage test with 5 ms increment. In general, 5 ms exposure time was sufficient to collect high-quality spectral data while the exposure time of 20 ms is used to compare and highlight the difference in radiation sensitivity.

Two main spectral changes occur due to radiation damage, a change in mass and a change in the spectra due to chemical reactions in the materials. The mass loss or gain of carbon, can be quantified by investigating changes of the carbon post edge at 330 eV. The most prominent effect was observed in the water-, cycloamine-based epoxy- and Spurr-based sample preparation approaches (Table 1). Interestingly, a positive mass change of carbon was observed in the sulphur embedding approach, which indicates deposition of carbon-containing species from the surrounding atmosphere onto the sample. In the high-vacuum chamber outgassing can occur from both sample and

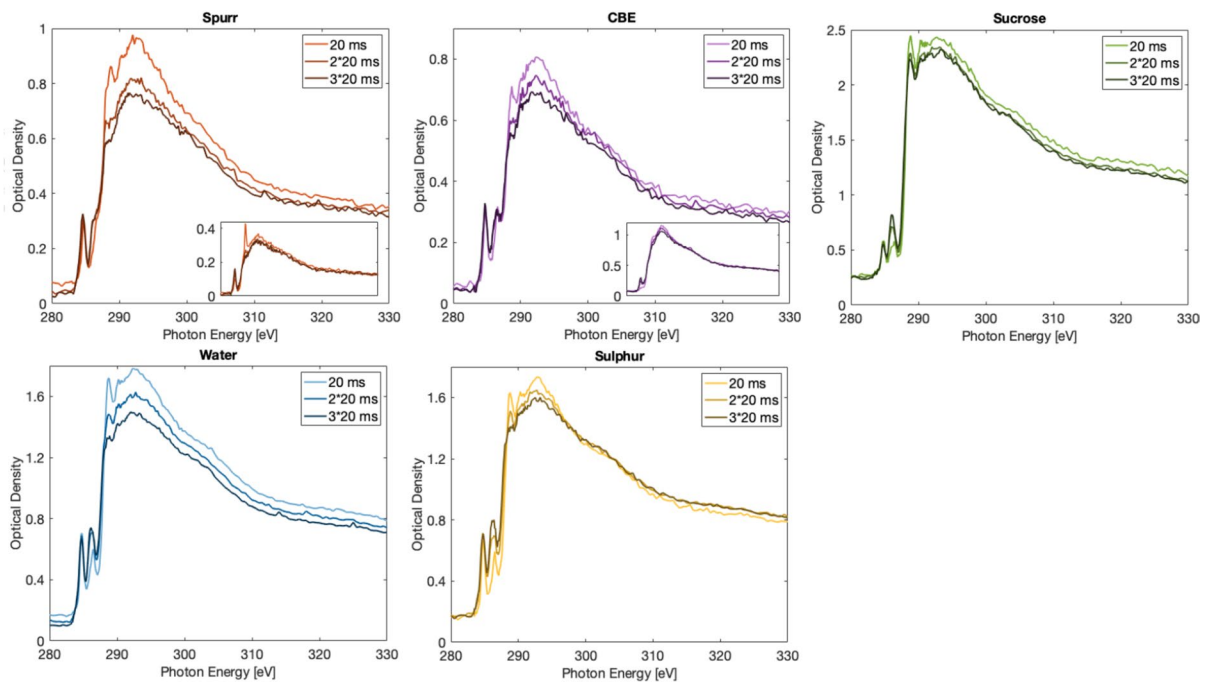


**Fig. 5** Radiation damage test of the samples with different embedding. Each time increment is 20 ms, the insets show radiation damage tests for the pure epoxies without any fibres

**Table 1** Optical densities at the post-edge (330 eV) of the same region of a fibre after 20 and 60 ms beam exposure in the different embeddings

	Spurr	Cycloamine-based epoxy	Sucrose	Water	Sulphur
OD <sub>330 eV</sub> 20 ms exposure	0.35	0.30	1.18	0.78	0.79
OD <sub>330 eV</sub> 3*20 ms exposure	0.31	0.27	1.12	0.71	0.81
Percentage of mass change	-11.4%	-10%	-5.08%	-8.97%	+2.53%

The percentage mass change is calculated by the ratio of the difference in optical densities between 20 and 60 ms and 20 ms

material in the chamber which may lead to redeposition of evaporated material by the incident beam.

Spectral changes due to beam exposure can be evaluated by comparing the relative change in intensity of different spectral peaks which relates to the breakage or formation of different covalent bonds in the material. In the case of the cellulose fibres, three different covalent bonds were particularly sensitive to radiation damage, identified by a change in peak intensity corresponding to (1) the C 1  $s \rightarrow 1 \pi^*$  transition of the phenolic carbons at 286.5 eV, (2) the C 1  $s \rightarrow 1 \pi^*$  transition of carboxylic carbon at 288.7 eV and (3) the broad C 1  $s \rightarrow \sigma^*$  transition of aromatic and aliphatic carbons at 293 eV. To make a relative

evaluation of the changes of each peak, the optical density at peak height was divided by the optical density by the post edge at 330 eV, results are illustrated in a bar chart, Fig. 6, and values are found in Table S1.

At 286.5 eV, the peak height increases with exposure time due to radiation damage for all sample preparation protocols except for Spurr epoxy method where the peak could not be resolved due to spectral overlap. At 288.7 eV the peak heights are instead decreased for all sample preparation protocols. This is in line with previous studies, showing that chain scissoring of the C=O and succeeding formation of C=C bonds are common for radiation exposed

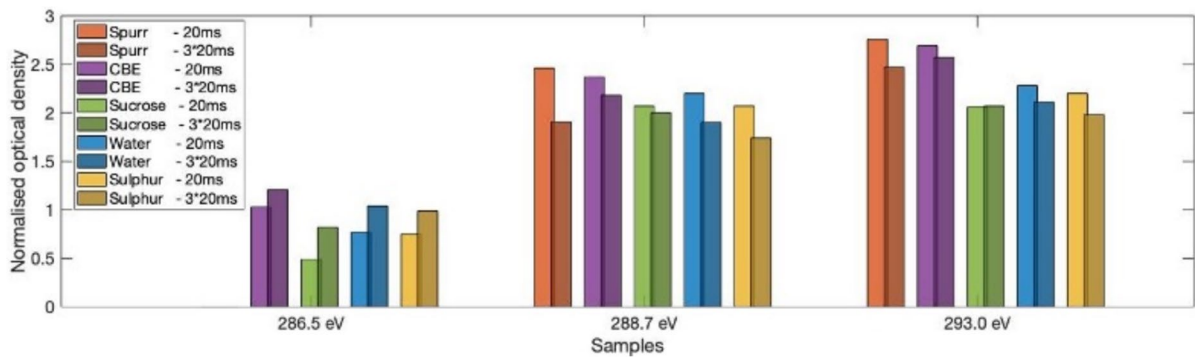


**Fig. 6** Bar chart showing the changes of the normalised optical density (NOD) of the spectral peaks at 286.5 eV, 288.7 eV and 293 eV for the fibres prepared with the different embeddings. The optical density is normalised relative to the post-edge (330 eV). The first measurement with 20 ms exposure

is shown in bright color and the second measurement with 3\*20 ms exposure is shown in dark color. The spectral signal at 286.5 eV cannot be resolved in the Spurr embedding due to the overlapping peaks of the epoxy

polymer samples (Zhang et al. 1995). The sample embedded in Spurr shows a significant decrease in peak intensity at both 288.7 eV and 293 eV. The strong reduction is likely a combination of damage to the fibre as well as damage to the embedding material as the neat Spurr embedding (Fig. 5e, inset) have a strong peak at 288.7 eV from its carboxylic carbon groups that disappears between the first and second 20 ms exposure. This highlights the high radiation sensitivity of the Spurr embedding, which is also reflected in the sample scan. In contrast, the cycloamine-based epoxy shows relatively smaller spectral changes compared to the other samples, suggesting that the epoxy may enhance radiation resistance and mitigate spectral alterations. However, a significant mass loss is still observed in this sample. Performing radiation damage tests on the pure epoxy confirms having less spectral changes in the cycloamine-based epoxy compared to the Spurr epoxy (Fig. S3, table S2, table S3). Note that the spectral changes in the sucrose sample protocol of the peaks at 288.7 and 293 eV are relatively small while a clear decrease in the peak at 286.5 eV is seen. We believe that this is due to that sucrose has a large spectral overlap with the fibres at these energies and that sucrose is less sensitive to radiation damage compared to the fibres.

In general fibres in all sample preparation strategies display some radiation damage, emphasising the need for efficient measurement strategies. The severity of radiation damage is increased by the radiation dose on the sample which is related to a high photon

flux, long exposure times and a focused X-ray beam, and is particularly severe around the carbon K-edge since absorption is high. Good measurement strategies to avoid radiation damage are thereby decreasing exposure time, the number of energies measured, or defocusing the X-ray beam as will be discussed in more detail in the following section.

#### Data collection strategies

Optimising data collection in spectro-microscopy requires balancing high spectral and spatial resolution while minimising radiation damage and measurement time. To achieve this, the acquisition strategy needs to be adapted to the goals of the experiment and the samples investigated. Below we provide guidelines for how data can efficiently be collected during an initial experiment for analysis of cellulose fibres.

At the start of an experiment, ensuring reliable data collection with the chosen experimental settings is crucial. This can be done by evaluating the full NEXAFS spectrum of the sample, performing a radiation damage check, and collecting reference spectra for components of the sample system. To collect a full NEXAFS spectra of the sample, an efficient approach is to perform a line scan across a sample edge, including an adjacent empty region. A line scan is preferred as it distributes the radiation dose over a larger sample area and in-sample variations can be accounted for. The method allows for simultaneous measurement of the sample

transmission and the incident beam intensity by the empty region. Measuring the incident beam is essential for generating accurate NEXAFS spectra, as it enables the conversion of raw transmission signals at specific energies into the optical density of the sample. However, the incident beam energy fluctuates slightly over time and is sensitive to substrate position, which can affect the background signal. Collecting the incident beam within the same scan helps minimise such errors. If an empty region cannot be included in the measurement, a separate scan should be performed in a nearby empty region as close in time and position as possible to account for the small variations in the incident beam. For epoxy embeddings, large sample sections are often achieved which is advantageous for imaging, however, it can also make it more difficult to create accurate spectra as empty regions are more sparsely located on the substrate. The full energy NEXAFS spectra acquired can be used for assessing which resonance energies are present in the sample. In addition, the optical density calculation indicates if the sample thickness is appropriate, where the general recommendation is to have a maximum optical density value around 1 in the spectrum. If the sample is too thick the incident beam is mainly absorbed resulting in poor data quality. If the sample is too thin the spectrum can appear noisy due to weak signal-to-noise ratio, making it difficult to extract meaningful chemical information (Watts et al. 2022).

A radiation damage check can be performed by repeating line scans in the same position of the sample. The goal of the radiation damage check is to detect when chemical changes and mass loss due to X-ray exposure occur and decide on suitable exposure times. Since the beam focus influences the dose received by the sample, this test should be performed using the same beam size intended for the actual measurements to ensure a realistic comparison. Alternatively, a highly focused beam can be used to determine the maximum tolerable dose, ensuring that exposure during measurements remains within a reasonable range. To minimise radiation damage during the entire experiment, it is advisable to use a defocused beam when scanning the sample plate to identify regions of interest before acquiring high-resolution data. Such overview scans should preferably be conducted at the post-edge energy or another energy

with lower sample absorption to reduce the radiation damage on the sample before acquiring the key measurements.

It is also advisable to collect reference spectra for the material system. The full NEXAFS spectra can be analysed as a linear combination of the individual chemical components, and having references for such components will contribute to a better understanding of the spectra and help towards quantitative analysis. Since biopolymer composition varies depending on the plant source, using specific reference materials improves accuracy. Furthermore, if an epoxy is used during sample preparation it is advisable to include reference spectra of pure epoxy, aiming to see at which energies there is spectral overlap between the epoxy and the sample. However, collecting reference spectra might not be possible in all sample cases, but still allows for quantitative assessment. Two of the most common analysis strategies are to apply singular value decomposition (SVD) (Koprinarov et al. 2002) and principal component analysis (PCA) combined with cluster segmentation (Lerotic et al. 2004, 2005) where PCA can be applied without available reference spectra or in the case of unknown component spectra. With PCA, the spectrum is estimated with the fewest possible virtual spectra that satisfactorily describe the observed variance in the images of the energy stack (Marcus 2023). The results do not yield a deconvolution of the spectrum but can be used to make a segmentation of domains with similar chemical composition. With SVD the known spectra of the pure components are used to perform a least square fit of the spectral contribution in each point, which provides a compositional map of the fraction of each species over the images in the energy stack. For more detailed description of data analysis and data treatment the reader is referred to reviews on the topic (Urquhart et al. 1999; Watts et al. 2006; Marcus 2023).

Once exposure limits have been determined and representative spectra have been collected, different data acquisition approaches can be taken to image the sample. In general, there are three main approaches (Willmott 2011): 1) *Imaging mode*, where the beam energy is fixed while the sample is raster scanned over the beam. This mode prioritises high spatial resolution and can efficiently map large areas of a sample to create a distribution map of the chemical species that has high absorbance at the chosen energy.

2) *Spectral mode*, where a scan is collected across the sample while the energy is varied over the carbon edge to provide the full NEXAFS spectrum. This mode prioritises collecting the sample absorption at a high number of energies within a large energy range to provide the most comprehensive data for determining chemical composition. 3) *Energy stacking mode*, where a sample is raster scanned over the beam like in imaging mode but at a few selected energies which correspond to resonance energies within the sample where absorption is strong for the components of interest. The acquisition of multiple energies provides

a compromise between imaging and chemical evaluation as it allows for chemical quantification while imaging still can be performed across larger sample areas due to collection of fewer energy points. Combining energy stacking and spectral mode is often advantageous as illustrated in Fig. 7. Energy stacking at a few selected energies provides high spatial details across the fibre (Fig. 7a), but results in low details of the energy spectra (Fig. 7c). In contrast, collecting a full energy spectra (Fig. 7d) with a lower spatial resolution (Fig. 7b) allows for detailed spectral analysis across the same sample region, making spectral

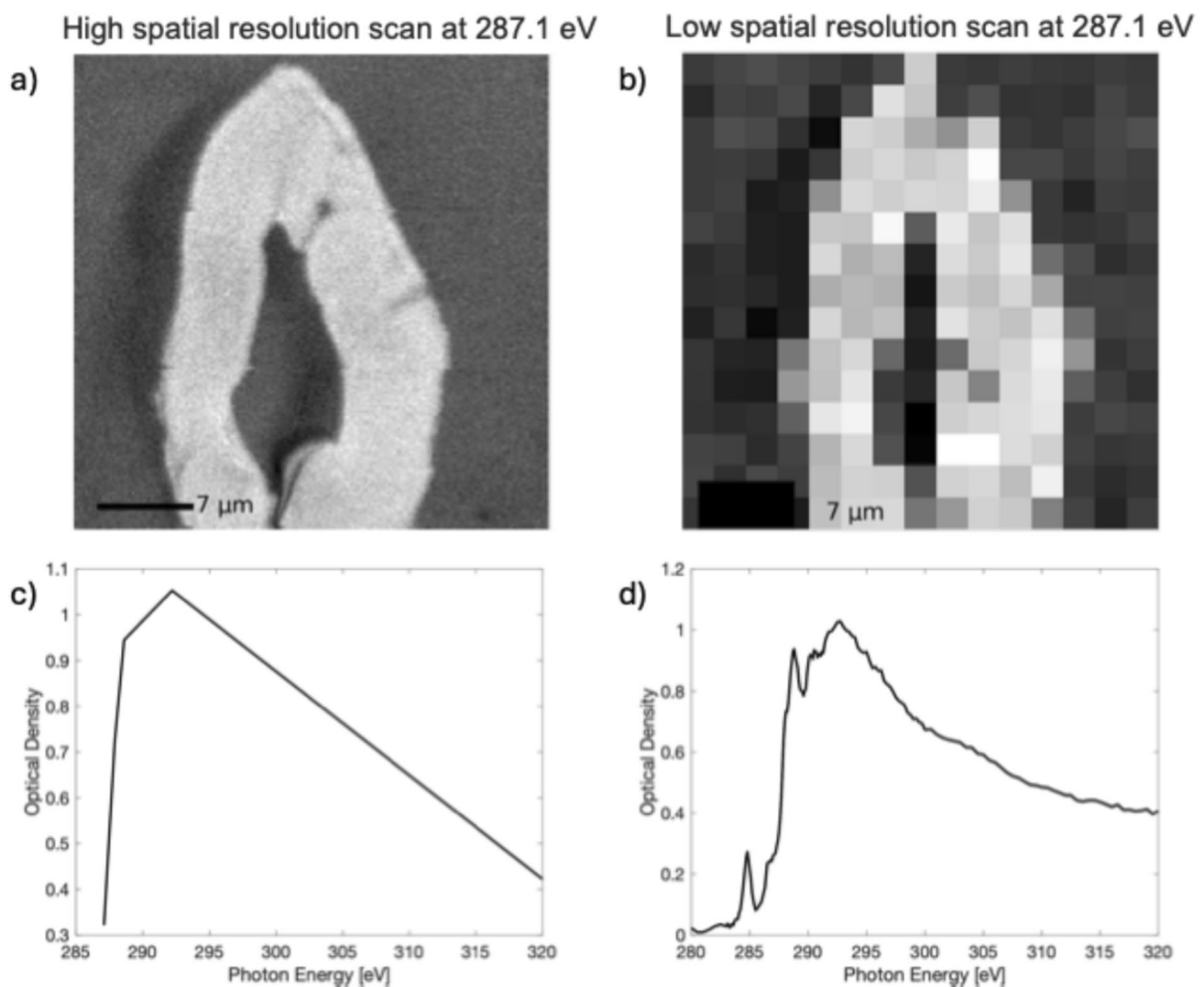


**Fig. 7** a, b STXM images collected at 287.1 eV of a cross section of a fibre and c, d corresponding averaged NEXAFS spectra. The figure illustrates a measurement where the spatial resolution was optimized by a highly focused beam, with the compromise of fewer energy scans (a, c) and a measure-

ment where the energy resolution over the fibre was optimized and instead the spatial resolution was compromised by using a defocused beam to collect the average absorption signal over the fibre providing the entire energy spectra of the cross section of the fibre (b, d)

interpretation more reliable. This approach enables both high spatial and high energy resolution across a large sample area while minimising measurement time and radiation damage. A key consideration when performing measurements at resonance energies is to include a post-edge measurement to correct for thickness variations, which affect absorption intensity across the energy range.

#### Overall performance of the different sample preparation strategies

Table 2 shows a summary of the discussed pros and cons of the different sample preparation strategies. For the practical sectioning, epoxy embedding strategies are superior as it enables sectioning with homogenous thickness in large sections. It also enables greater control of the orientations of fibres in the cuts compared to the other methods. However, epoxy embeddings are carbon-based compounds which will result in strong spectral contributions around the carbon K-edge, which can give overlapping contributions to the spectral signals. Depending on the feature of interest in the investigated sample, different chemical compositions of the embedding materials can be selected to minimise the spectral overlap between the embedding material and the species of interest to

provide a way of identifying and mapping the component within the sample. For studying lignocellulose fibres, the cycloamine-based epoxy shows advantages compared to the Spurr epoxy due to less overlapping signals with the lignin in the material and lower sensitivity to radiation damage.

In addition to epoxy-based methods, water and sucrose solutions were used as a cryo-embedding. The advantage with sucrose solution compared to water solution is that for sensitive samples it reduces the risk for crystal formation during freezing which can fracture and damage the samples. However, the almost identical chemical structure of sucrose and cellulose creates highly overlapping signals in the absorption spectrum. The sectioning of water embedded samples where challenging, but the resulting sections were still similar between sucrose and water-embedded samples. It was therefore deemed more advantageous to use water as embedding media in the cryo-embedding sample preparation protocols.

Lastly, an embedding of elemental sulphur was investigated, which in similarity to cryo-embedding with water does not result in any spectral overlap between the sample and the embedding material. However, the elemental sulphur presented other challenges, including a poor adhesion to the substrate which resulted in fibres falling off the substrate during

**Table 2** Overview of the identified advantages and challenges with the different preparation strategies

Sample preparation protocol	Pros	Cons
Elemental sulphur	<ul style="list-style-type: none"> <li>- No spectral overlap with cellulose and lignin</li> <li>- Adequate mechanical properties for sectioning</li> </ul>	<ul style="list-style-type: none"> <li>- Poor adhesion to sample substrate</li> <li>- Difficult to section with homogenous thickness</li> </ul>
<i>Cryo-embedding strategies</i>		
Water	<ul style="list-style-type: none"> <li>- No spectral overlap with cellulose and lignin</li> </ul>	<ul style="list-style-type: none"> <li>- Fibre aggregation</li> <li>- Difficult to section</li> </ul>
Sucrose	<ul style="list-style-type: none"> <li>- Reduce potential sample damage crystal formation upon freezing</li> </ul>	<ul style="list-style-type: none"> <li>- Fibre aggregation</li> <li>- Difficult to section with homogenous thickness</li> <li>-Spectral overlap with cellulose fibres</li> </ul>
<i>Epoxy embedding strategies</i>		
Cycloamine-based epoxy	<ul style="list-style-type: none"> <li>- Good mechanical properties for sectioning</li> <li>- Less sensitive to spectral changes from radiation damage</li> </ul>	<ul style="list-style-type: none"> <li>- Spectral overlap with cellulose fibres</li> <li>- Difficult to identify fibres within sections</li> <li>- Collection of reference measurements of incident beam may be more difficult</li> </ul>
Spurr	<ul style="list-style-type: none"> <li>- Good mechanical properties for sectioning</li> </ul>	<ul style="list-style-type: none"> <li>- Spectral overlap with cellulose fibres</li> <li>- Difficult to identify fibres within sections</li> <li>- Collection of reference measurements of incident beam may be more difficult</li> </ul>

measurements when exposed to the high vacuum in the measurement chamber. We hypothesise that this effect can be mitigated by either coating the silicon nitride support membrane with a conductive material, such as graphene or a thin metal layer, or sandwiching the fibre samples between two separate support membranes to provide mechanical stability. Another option is to store the sample at low temperature to slow down the depolymerisation of the sulphur to reduce the evaporation rate. The embedding process using elemental sulphur was more time-consuming compared to the epoxy embeddings and the resulting sections varied in thickness.

## Conclusion

In this work we show how fibre-based cellulose materials can be characterised with X-ray spectro-microscopy to reveal the distribution of chemical composition of the material. Key to successful experiments is sample preparation and an efficient measurement strategy to minimise radiation damage. Preparing the thin sections needed to image fibres with soft X-ray spectro-microscopy at the carbon K-edge is challenging. The different sample preparation strategies studied in this work reveal advantages as well as challenges for various aspects of the measurements. For the sectioning, the epoxy embeddings are the prime alternative for homogenous sections of larger areas, which is highly advantageous for imaging. However, carbon-based epoxies may result in contributions to the spectral signal of the samples which complicates the chemical analysis of the material. As an alternative water embedding does not contribute with any spectral signal around the carbon K-edge, but it is instead more difficult to mechanically section, and the fibres tend to aggregate which makes it more difficult for imaging purposes. Sulphur embedding presents an embedding strategy which both enables adequate mechanical properties for sectioning and at the same time does not contribute with overlapping signals. Hence it is advantageous for both spectral and imaging analysis, although poor adhesion to the substrate present challenges for measurements as it risks falling of the membrane. In conclusion the choice of the best preparation strategy for a certain experiment needs to be determined based on the nature of the sample and the goal of the measurement. We showcase the

method here with the imaging of a single TMP fibre where we show that one can spatially separate different lignin composition. This illustrates the high chemical sensitivity of the technique for spatially resolving small chemical changes and present opportunities to study modifications in fibres in more detail.

**Acknowledgments** The authors acknowledge the Paul Scherrer Institute, Villigen, Switzerland for provision of synchrotron radiation beamtime at the beamline Pollux of the SLS. We gratefully acknowledge Umea Centre for Electron Microscopy for assisting with the sample preparation.

**Author Contribution** L.B., M.O., and M.L. conceptualized the study and planned the beamtime. G.W. synthesized the samples used in the study. L.B. and A.Z. prepared the sample embeddings and performed sample cutting. L.B., M.O., J.A., M.L., performed synchrotron measurements and B.W. acted as the beamline scientist and provided technical support. L.B., M.O. analyzed the data, and wrote the first draft of the manuscript, where M.L. and B.W. assisted interpreting data. M.L. and A.M. supervised the study. All authors reviewed and provided feedback on the manuscript and approved it for submission.

**Funding** Open access funding provided by Chalmers University of Technology. LB has been funded by the competence center FibRe–Design for Circularity: supported by the Swedish Innovation Agency Vinnova (grant number 2019–00047) and by the industrial partners in FibRe. The authors also acknowledge financial support by Chalmers Gender Initiative for Excellence (Genie). MO has been funded by the Area of Advance Nano at Chalmers University of Technology through an excellence initiative PhD student position.

**Data Availability** The datasets generated and analysed during the current study are available from the corresponding author on reasonable request.

## Declaration

**Conflict of interest** The authors declare no competing interests.

**Open Access** This article is licensed under a Creative Commons Attribution 4.0 International License, which permits use, sharing, adaptation, distribution and reproduction in any medium or format, as long as you give appropriate credit to the original author(s) and the source, provide a link to the Creative Commons licence, and indicate if changes were made. The images or other third party material in this article are included in the article's Creative Commons licence, unless indicated otherwise in a credit line to the material. If material is not included in the article's Creative Commons licence and your intended use is not permitted by statutory regulation or exceeds the permitted use, you will need to obtain permission directly from the copyright holder. To view a copy of this licence, visit <http://creativecommons.org/licenses/by/4.0/>.

## References

- Adler E (1977) Lignin chemistry—past, present and future. *Wood Sci Technol* 11:169–218. <https://doi.org/10.1007/BF00365615>
- Beetz T, Jacobsen C (2003) Soft X-ray radiation-damage studies in PMMA using a cryo-STXM. *J Synchrotron Radiat* 10:280–283. <https://doi.org/10.1107/s0909049503003261>
- Coffey T, Sg U, Ade H (2002) Characterization of the effects of soft X-ray irradiation on polymers. *J Electron Spectrosc Relat Phenom* 122:65–78. [https://doi.org/10.1016/S0368-2048\(01\)00342-5](https://doi.org/10.1016/S0368-2048(01)00342-5)
- Dazzi A, Prater Cb (2017) AFM-IR: technology and applications in nanoscale infrared spectroscopy and chemical imaging. *Chem Rev* 117:5146–5173. <https://doi.org/10.1021/acs.chemrev.6b00448>
- Akin De, Eder M, Burgert I, Müssig J, Slotmaker T (2010). *Industrial Applications of Natural Fibres* 11–48. Wiley. <https://doi.org/10.1002/9780470660324.ch2>
- Deslattes Rd, Kessler Eg, Indelicato P, De Billy L, Lindroth E, Anton J (2003) X-ray transition energies: new approach to a comprehensive evaluation. *Rev Mod Phys* 75:35–99. <https://doi.org/10.1103/RevModPhys.75.35>
- Frommherz U, Raabe J, Watts B, Stefani R, Ellenberger U (2010) Higher Order Suppressor (HOS) for the PoLux Microspectroscopy Beamline at the Swiss Light Source SLS. *AIP Conf Proc* 1234:429–432. <https://doi.org/10.1063/1.3463232>
- Fromm J, Rockel B, Lautner S, Windeisen E, Wanner G (2003) Lignin distribution in wood cell walls determined by TEM and backscattered SEM techniques. *Journal of Structural Biology* 143(1):77–84. [https://doi.org/10.1016/S1047-8477\(03\)00119-9](https://doi.org/10.1016/S1047-8477(03)00119-9)
- Hosseini S, Venkatesh A, Boldizar A, Westman G (2021) Molybdenum disulphide—a traditional external lubricant that shows interesting interphase properties in pulp-based composites. *Polym Compos* 42:4884–4896. <https://doi.org/10.1002/pc.26197>
- Kangas H, Suurnäkki A, Kleen M (2007) Modification of the surface chemistry of TMP with enzymes. *Nord Pulp Pap Res J* 22:415–423. <https://doi.org/10.3183/npprj-2007-22-04-p415-423>
- Karunakaran C, Christensen Cr, Gaillard C, Lahlali R, Blair Lm, Perumal V, Miller Ss, Hitchcock Ap (2015) Introduction of soft X-ray spectromicroscopy as an advanced technique for plant biopolymers research. *PLoS ONE* 10:e0122959. <https://doi.org/10.1371/journal.pone.0122959>
- Koprinarov I, Hitchcock A, Mccrory C, Childs R (2002) Quantitative mapping of structured polymeric systems using singular value decomposition analysis of soft X-ray images. *J Phys Chem B* 106:5358–5364. <https://doi.org/10.1021/jp013281l>
- Lahtinen Mh, Ojala A, Wikström L, Nättinen K, Hietala S, Fiskari J, Kilpeläinen I (2021) The impact of thermomechanical pulp fiber modifications on thermoplastic lignin composites. *Compos Part C Open Access* 6:100170. <https://doi.org/10.1016/j.jcomc.2021.100170>
- Lehmann J, Liang B, Solomon D, Lerotic M, Luizão F, Kinyangi J, Schäfer T, Wirick S, Jacobsen C (2005) Near-edge X-ray absorption fine structure (NEXAFS) spectroscopy for mapping nano-scale distribution of organic carbon forms in soil: Application to black carbon particles. *Global Biogeochemical Cycles* 19. <https://doi.org/10.1029/2004GB002435>
- Lerotic M, Jacobsen C, Schäfer T, Vogt S (2004) Cluster analysis of soft X-ray spectromicroscopy data. *Ultramicroscopy* 100:35–57. <https://doi.org/10.1016/j.ultramic.2004.01.008>
- Lerotic M, Jacobsen C, Gillow J, Francis A, Wirick S, Vogt S, Maser J (2005) Cluster analysis in soft X-ray spectromicroscopy: finding the patterns in complex specimens. *J Electron Spectrosc Relat Phenom* 144:1137–1143. <https://doi.org/10.1016/j.elspec.2005.01.158>
- Lerotic M, Mak R, Wirick S, Meirer F, Jacobsen C (2014) MANTiS: a program for the analysis of X-ray spectromicroscopy data. *J Synchrotron Radiat* 21:1206–1212. <https://doi.org/10.1107/S1600577514013964>
- Marcus Ma (2023) Data analysis in spectroscopic STXM. *J Electron Spectrosc Relat Phenom* 264:147310. <https://doi.org/10.1016/j.elspec.2023.147310>
- Mertens O, Gurr J, Krause A (2017) The utilization of thermomechanical pulp fibers in WPC: A review. *Journal of Applied Polymer Science* 134. <https://doi.org/10.1002/app.45161>
- Mleziva MM, Wang JH (2012) 10.23 - Paper. *Polymer science: a comprehensive reference*. 10:397–410. <https://doi.org/10.1016/B978-0-444-53349-4.00274-0>
- Noguchi T, Takase M, Matsumoto R, Kebukawa Y, Suga H, Kondo M, Takahashi Y, Takeichi Y, Yabuta H (2020) An another protocol to make sulfur embedded ultrathin sections of extraterrestrial small samples. *Life* 10:135. <https://doi.org/10.3390/life10080135>
- Raabe J, Tzvetkov G, Flechsig U, Böge M, Jaggi A, Sarafimov B, Vernooij M, Huthwelker T, Ade H, Kilcoyne D, Tyliszczak T, Fink Rh, Quitmann C (2008) PoLux: a new facility for soft x-ray spectromicroscopy at the Swiss Light Source. *Rev Sci Instrum*. <https://doi.org/10.1063/1.3021472>
- Späth A, Meyer M, Semmler S, Fink Rh (2015) Microspectroscopic soft X-ray analysis of keratin based biofibers. *Micron* 70:34–40. <https://doi.org/10.1016/j.micron.2014.12.003>
- Studel R, Eckert B, Steudel Y, Wong M, Krossing I, Kleinnan W, Keizer A, Janssen A. *Elemental Sulfur and Sulfur-Rich Compounds, Part 1*. (2003). <https://doi.org/10.1007/b12115>
- Urquhart Sg, Hitchcock Ap, Smith Ap, Ade Hw, Lidy W, Rightor Eg, Mitchell Ge (1999) NEXAFS spectromicroscopy of polymers: overview and quantitative analysis of polyurethane polymers. *J Electron Spectrosc Relat Phenom* 100:119–135. [https://doi.org/10.1016/S0368-2048\(99\)00043-2](https://doi.org/10.1016/S0368-2048(99)00043-2)
- Wang J, Morin C, Li L, Ap H, Scholl A, Doran A (2009) Radiation damage in soft X-ray microscopy. *J Electron Spectrosc Relat Phenom* 170:25–36. <https://doi.org/10.1016/j.elspec.2008.01.002>
- Watts B, Ade H (2012) NEXAFS imaging of synthetic organic materials. *Mater Today* 15:148–157. [https://doi.org/10.1016/S1369-7021\(12\)70068-8](https://doi.org/10.1016/S1369-7021(12)70068-8)
- Watts B, Thomsen L, Pc D (2006) *Methods in carbon K-edge NEXAFS: experiment and analysis*. *J Electron Spectrosc*

- Relat Phenom 151:105–120. <https://doi.org/10.1016/j.elspec.2005.11.006>
- Watts B, Finizio S, Raabe J (2022) Quantifying signal quality in scanning transmission X-ray microscopy. *Synchrotron Radiation* 29:1054–1064. <https://doi.org/10.1107/S1600577522004210>
- Willmott P (2011) *An introduction to synchrotron radiation: techniques and applications*. John Wiley & Sons. <https://doi.org/10.1002/9781119970958>
- Zhang X, Jacobsen C, Lindaas S, Williams S (1995) Exposure strategies for polymethyl methacrylate from in situ x-ray absorption near edge structure spectroscopy. *Journal of Vacuum Science, Technology b: Microelectronics and Nanometer Structures Processing, Measurement, and Phenomena* 13:1477–1483. <https://doi.org/10.1116/1.588175>
- Zhang W, Melo L, Hitchcock Ap, Bassim N (2019) Electron beam damage of epoxy resin films studied by scanning transmission X-ray spectromicroscopy. *Micron* 120:74–79. <https://doi.org/10.1016/j.micron.2019.02.003>

**Publisher's Note** Springer Nature remains neutral with regard to jurisdictional claims in published maps and institutional affiliations.